**Atmospheric
Measurement
Techniques
Discussions**

Meteorological information in GPS-RO reflected signals

K. Boniface[1], J. M. Aparicio[1], and E. Cardellach[2]

[1]Data Assimilation and Satellite Meteorology, Environment Canada, Dorval, QC, Canada
[2]Institute of Space Sciences, ICE-CSIC/IEEC, Barcelona, Spain

Correspondence to: K. Boniface (karen.boniface@ec.gc.ca)

AMTD

4, 1199–1231, 2011

Meteorological information in GPS-RO reflected signals

K. Boniface et al.

Title Page

Abstract	Introduction
Conclusions	References
Tables	Figures

|◄ | ►|
◄ | ►
Back | Close

Full Screen / Esc

Printer-friendly Version

Interactive Discussion

Abstract

Vertical profiles of the atmosphere can be obtained globally with the radio-occultation technique. However, the lowest layers of the atmosphere are less accurately extracted. A good description of these layers is important for the good performance of Numeri-
cal Weather Prediction (NWP) systems, and an improvement of the observational data available for the low troposphere would thus be of great interest for data assimilation. We outline here how supplemental meteorological information close to the surface can be extracted whenever reflected signals are available. We separate the reflected signal through a radioholographic filter, and we interpret it with a ray tracing procedure,
analyzing the trajectories of the electromagnetic waves over a three-dimensional field of refractive index. A perturbation approach is then used to perform an inversion, identifying the relevant contribution of the lowest layers of the atmosphere to the properties of the reflected signal, and extracting some supplemental information to the solution of the inversion of the direct propagation signals. The methodology is applied to one
reflection case.

1 Introduction

The measurement and interpretation of GPS radio occultation signals (GPS-RO) that have suffered only atmospheric refraction during their propagation is well established. This includes their description as propagating waves, and therefore the presence of
diffraction. The analysis of such signals, and in particular of radio occultation data is of great interest for planetary atmospheres (Fjeldbo et al., 1971), Earth's atmospheric experimental and theoretical studies (Kursinski et al., 1996; Sokolovskiy, 1990; Gorbunov, 1988; Gurvich et al., 1982) and ionospheric studies (Raymund et al., 1990; Hajj et al., 1994). Indeed, beyond the geometric delay due to the finite speed of light, the
delay in excess of this quantity contains information about the amount and distribution

of matter encountered during the propagation, such as dry air and moisture in the atmosphere, and their gradients.

Over the last decades a number of studies have assessed the geophysical content of Global Postionning System (GPS) signals reflected off the surface of the Earth (Beyerle et al., 2002; Cardellach et al., 2008). To the presence of refraction, and eventually diffraction, this adds reflection. We will hereafter name as *direct*, the signals whose propagation is determined mainly by refraction phenomena, and eventually diffraction. We will instead name as *reflected*, the signals whose propagation involves critically some reflection in the surface, therefore introducing a qualitative difference with respect to the direct signals. Reflected signals are of course subject to refraction as well.

Reflected signals probe the entire atmosphere, down to the surface. This leaves an atmospheric signature. In principle, the reflection itself may as well leave a signature in the signal, therefore obscuring the interpretation of the collected signal exclusively in terms of atmospheric properties. We have then limited here to the specific case where the signal bounces over the ocean, which is at a known altitude. At incidence angles closer to normal, the surface roughness, which is essentially determined by the presence of waves, is several times larger than the signal wavelength, and this can easily produce decoherence in the GPS signal. Coherence, however, is critical for all phase-based analyses of GPS signals, including GPS-RO. However, at near grazing incidence, the vertical scale that determines if close propagation paths are coherent is the Fresnel diameter of the propagation beam, which for paths near the surface is of several hundred meters. Surface waves are much smaller than this. Therefore, at these incidence angles, the reflected signal does not loose coherence due to the presence of surface waves.

Our attention is particularly dedicated to an improved description of the lowest layers of the atmosphere, were the inversion of direct GPS-RO signals is less accurate and subject to bias (Ao et al., 2003; Sokolovskiy et al., 2009). The refractivity bias in GPS occultation retrievals is related to the presence of strong vertical gradients of refractivity, mostly between the surface and the boundary layer. These strong gradients may cause

Meteorological information in GPS-RO reflected signals

K. Boniface et al.

superrefraction, or bend the signal outside the orbital segment where the receiver is active. In either case, there is a lack of information concerning these layers. The potential of GPS-RO data has already been analyzed in numerous global data assimilation experiments, and its geophysical data succesfully extracted from the analysis of direct
5 propagation paths. These data are routinely used in operational Numerical Weather Prediction (NWP) systems (Healy, 2008; Cucurull et al., 2006; Aparicio and Deblonde, 2008; Rennie, 2010; Poli, 2008).

The main objective of the study is to assess the potential of GPS-RO signals that rebound off the ocean surface. Reflected signals propagate following different geometries
10 than the direct signals, and traverse atmospheric layers at different incidence angles. This may allow them to traverse layers that are superrefractive at a more grazing incidence. There is therefore a potential to extract additional information with respect to the direct signals. Given that information describing the low troposphere is the most difficult to extract with direct propagation GPS-RO, and that information concerning these
15 layers is the most valuable, we consider this potential worth exploring.

We will first use a radio-holographic technique to identify the propagation paths. Reflected signals present in GNSS occultation data present different frequency spectra than the direct signals (Beyerle et al., 2002; Cardellach et al., 2008). This allows a separation of both, and further independent treatment as data sources. For the inter-
20 pretation, we use a numerical model based on ray tracing, where propagation trajectories of electromagnetic waves are evaluated over a given (a priori) three dimensional field of refractive index. Supplemental information is also evaluated to allow a perturbation analysis. This latter describes the dependence of the raytracing result with respect to variations of the apriori field. The perturbation analysis allows a least squares fit to
25 the observed reflected data, which retrieves a correction to the apriori refractivity field.

Title Page

Abstract | Introduction

Conclusions | References

Tables | Figures

◄ | ►

◄ | ►

Back | Close

Full Screen / Esc

Printer-friendly Version

Interactive Discussion

2 Radio-holographic analysis to separate direct and reflected signals

One possible procedure for the separation of the direct and reflected signals is a radio holographic analysis (Hocke et al., 1999). Signal to noise ratios (SNR), a measure of signal amplitude, hereafter expressed as $A(t)$, and carrier phase measurements $\varphi(t)$ have been recorded at a number of sample instants t. As an example, we show in Fig. 1, the SNR for both signals L1 and L2 during a setting occultation (COSMIC C001.2007.100.00.29.G05, where COSMIC is for Constellation Observing System for Meteorology Ionosphere and Climate: see Rocken et al., 2000 for system description), as given by the GPS receiver. The signal is clearly detected during approximately 80 s. Then the SNR for L1 and L2 become almost zero.

To realize the radiohologram power spectrum derived from a GPS occultation, $A(t)$ and carrier phase measurements are combined into a complex electric field $E(t)$, expressed as follows:

$$E(t) = A(t) \, e^{i\varphi(t)} \tag{1}$$

We will also construct a reference electric field (see Cardellach et al., 2004 for more details):

$$E_\mathrm{F}(t) = A_\mathrm{F}(t) \, e^{i\varphi_\mathrm{F}(t)} \tag{2}$$

We choose the amplitude and phase of this reference field to our convenience. The measured field can then be expressed relative to this reference:

$$E(t) = B(t) \cdot E_\mathrm{F}(t) = A(t)/A_\mathrm{F}(t) \, e^{i(\varphi(t)-\varphi_\mathrm{F}(t))} \cdot E_\mathrm{F}(t) \tag{3}$$

If the reference field $E_\mathrm{F}(t)$ is judiciously chosen, the measured field can be expressed with a slowly varying complex (beating) function $B(t)$. Once the behavior with larger frequency has been separated, a frequency analysis of $B(t)$ will show how $E(t)$ departs from the reference field, hopefully containing only low frequency components. We will

1203

call radiohologram to a sliding Fourier Transform (FT) analysis of $B(t)$. This can help describing the internal structure of the signal, and identifying several close but distinct subcarriers within the signal. Depending on the circumstances, the existence of these subcarriers may be associated with the presence of multipath, the vertical structure of
5   the propagation beam, or the existence of a reflection (Melbourne, 2004).

Since, in the case of COSMIC receivers, the sampling is done at 50 Hz, this Fourier analysis can only explore a bandwith of 50 Hz around the reference field. It can therefore only be useful if the reference signal has been tuned to the target of study to better than 50 Hz. The GRAS receiver can sample and record at 1 kHz, and this pro-
10 cedure could explore a bandwidth of 1 kHz around the reference field. Figure 2 shows the temporal evolution (x-axis) of the hologram's power spectrum of a COSMIC occultation. The vertical axis represents the shifts in frequency with respect to the reference field. Time is measured since the beginning of the occultation. The reference field was chosen to mimic the main frequency component of the direct signal ($E_F(t)$ is a sliding
15 average of $E(t)$, see Cardellach et al., 2010 for more details). Since the power of the direct signal is substantially larger, it dominates the smoothed function. Thus the direct signal appears in the hologram with nearly zero-frequency, broadened by atmospheric and ionospheric small scale structure.

During most of the occultation, the power received at frequencies far from this broad-
20 ened but clear direct signal has no structure evidently different from noise. Close to the surface touchdown of the direct signal, another component becomes evident. It is initially strongly aliased (much more than 25 Hz away from the direct signal), and also showing a large phase acceleration (its frequency changes). Both the phase acceleration and the frequency offset reduce, until this component finally merges with the
25 direct signal. It is possible to identify that this component is associated with a reflection, rather than some other form of multipath, by the agreement of the frequency behavior with respect to the theoretical behavior of a reflection (e.g. Beyerle and Hocke, 2001).

The radio holographic analysis, as a means to separate direct and reflected signal components is also discussed in Pavelyev et al. (1996) and Hocke et al. (1999). Once

identified that the component is a reflection, detailed analysis of the frequency shifts between direct and reflected signals can help determining atmospheric or surface properties. Complex patterns found in radio hologram spectra with a subset of observations at low latitudes are also been interpreted in terms of multipath propagation caused by layered structures in the refractivity field (Beyerle et al., 2002). Beyerle and Hocke (2001) also shows that GPS signals observed by the GPS/MET radio occultation experiment contain reflected signal components.

The frequency of the reference field is nearly that of the direct signal. The reflected signal has a substantial frequency shift in a large portion of the graph, several times larger than the bandwidth of 50 Hz. It is also worth mentioning that since the receiver is tracking the direct signal, and not the reflected one, this latter is detected, and produces the interference. We are trying to analyze this interference, only because it also matches the C/A pattern of the direct signal. There is no correlator in the receiver dedicated to track the reflected signal, and we depend on this interference to extract the properties of the reflection. This match in C/A code, however, occurs only if the relative delay between direct and reflected signals is smaller than 1 C/A chip, or 300 m (Parkinson and Spilker, 1996). The mismatch in optical lengths between both signals causes the reflected signal to be suboptimally detected, to only a fraction of its actual power. At 300 m or more of delay, it is detected with negligible power. Therefore, the reflected signal can only be extracted with the procedure mentioned if the optical path of both is less than 300 m apart. In Fig. 3, a raytracing estimation (see below, for more details of the raytracer) of the direct and reflected excess paths is shown. It can be seen that both signals are less than 1 C/A chip apart only during a fraction of the occultation, of the order of 20 s. It is therefore only during this time window that we can expect to extract data describing the reflected signal, and therefore any signature within it of the properties of the atmosphere.

3 Observables: the wrapped and unwrapped phases

Given a beating function $B(t) = E(t)/E_F(t)$, the hologram is its sliding Fourier Transform (FT):

$$H(t,f) = \mathcal{F}[B(t)] \tag{4}$$

In this case, it is interpreted that the *direct* signal is the power found at low frequency in the hologram, very close to the reference model, and the *reflected* signal, as the slant component, that appears aliased several times. We then select each of them applying some hologram mask D, that selects the direct signal, and a complementary mask $R = I - D$, where I is the identity. Since the objective of this study is to explore the geophysical content of the reflection, rather than a generic algorithmic definition of this mask, we have here selected R (and its complement D) conservatively, with an ad hoc definition of the slant area of the hologram. This should be refined into a more generic, and especially automatic, definition.

For the occultation profile studied here (COSMIC's C001.2007.100.00.29.G05) the reflection begins to be detectable around $t = 65$ s. The mask R is applied beginning at this time and with an orientation of its approximate phase acceleration ($0.52\,\mathrm{Hz\,s^{-1}}$). The mask is marked in the hologram with a red parallelogram (Fig. 2).

Reverting with inverse FT to the beating function space, the masks define two beating functions:

$$B_D(t) = \mathcal{F}^{-1}D[H(t, f)] \tag{5}$$

and

$$B_R(t) = \mathcal{F}^{-1}R[H(t, f)] \tag{6}$$

which we will identify as the beating functions of the separated direct and reflected signals. This eventually allows the reconstruction of the two components of the electromagnetic field. The separation cannot of course be carried out perfectly, as the

frequency of both signals is too close near their merging (around 75 s), or is aliased (e.g. around 60 s) into the direct signal. A receiver with higher sampling (such as GRAS) could separate better the two propagation channels.

It is here evident that a judicious choice of the reference field is critical, as otherwise no practical mask will separate the two components properly. This sliding mean is a reasonable choice, as the direct signal is substantially stronger than the reflected, dominating the mean and leaving the direct signal into a simple geometry: a straight line around zero frequency, with moderate broadening.

Each of the two beating functions $B_D(t)$ and $B_R(t)$ represents a slowly rotating phasor around the reference field $E_F(t)$. The phasors are known only modulo 2π, but could be unwrapped (reconnected) to continuous functions removing the jumps of 2π. The signal represented by $B_D(t)$ can be identified during most of the recording period, from 0 to 80 s. The phasor $B_D(t)$ is very similar to the beating function from the full recorded signal, as only a small amount of power has been removed. It is however free from most of the interference of the surface. In any case, we assume that the processing and interpretation of this component are standard practice, and we will not discuss it further.

The signal $B_R(t)$ has a significant amplitude only during a small portion of the occultation (55 s to 80 s). Regardless of the exact mask chosen, this could be expected for any reasonable mask since at earlier times the reflected signal was outside the C/A chip of the direct signal, and was ignored by the correlator. It is also a slow rotating phasor (slow compared to $E_R(t)$), although faster than $B_D(t)$, since the reference field is not tuned to follow this signal. It can also be reconnected, removing the 2π jumps, to form another signal, that we will interpret as the reflected signal.

The delays between the reconnected direct, reconnected reflected and reference signals, allows us to retrieve the equivalent excess of phase between any pair of them. On the left side, Fig. 4 shows the excess of phase obtained between the reflected signal and the reference one, that is, the phase of $B_R(t)$. We call this phasor the interferometric signal between both. The oscillations indicate the existence of a relative

rotation between the two signals by several turns (it is wrapped). The plot on the right side represents the same signal, with all 2π jumps removed. We will call this the un-wrapped interferometric signal, equivalent to relative delay between the reflected and the direct ray path, and it will be our primary observable for the extraction of atmo-
5   spheric properties.

4   Ray tracing analysis

Ray tracing is a numerical procedure that allows the evaluation of propagation trajec-tories of the electromagnetic waves. In this study we present a ray tracing procedure that allows the determination of the regions of the atmosphere that are being probed
10   by a given propagation beam. The ray tracing is computed between an emission point (transmitter, in general a GNSS satellite orbiting at heights of about 20 000 km) and a receiver point (here, a LEO satellite). It characterises the way the light propagates when moving through material media of varying refraction index.
       Wave propagation calculation can be done in two ways. The first is the geometri-
15   cal approach. Only the direction of propagation of electromagnetic is used. Signal propagation is thus reduced to the knowledge of rays characteristics and signal wave lengths. Signal characteristics are influenced by the change of refractivity across the material medium. In the second method, signal propagation can be represented as an ondulatory model, which is computationally more complex. In the case of GPS radio
20   occultation, the wave character of light is not negligible, but small: signal propagates as a beam of non-negligible width, of the order of the Fresnel diameter. Although not neg-ligibly so, the Fresnel diameter is moderately small with respect to other cross-beam length scales, such as the vertical structure of the atmosphere.
       However, for our main purpose, which is the identification of the interaction between
25   the beams and each layer of the atmosphere, this width is not critical, and we will neglect the wave nature of GPS signals in this first test. We will therefore describe light

Meteorological information in GPS-RO reflected signals

K. Boniface et al.

Title Page

Abstract	Introduction
Conclusions	References
Tables	Figures

|◄ | ►|

◄ | ►

Back | Close

Full Screen / Esc

Printer-friendly Version

Interactive Discussion

waves as propagating in a direction orthogonal to the geometrical wavefronts defined as the surfaces on which the signal phase is constant.

4.1 Ray path determination

The index of refraction, n in some medium is defined as the speed of light in vacuum divided by the speed of light in the medium. In the atmosphere, the index of refraction is very close to unity. Consequently, it is more common to express it in terms of refractivity N. By definition, $N = (n - 1) \times 10^6$.

Our final objective is to extract the unknown field of refraction index $n(\overrightarrow{x})$ from some form of measurement, or combination, of the optical lengths L_{obs} through different propagation paths.

The total optical length L of a given path p, can be expressed as:

$$L = \int_p n(\overrightarrow{x}) ds \qquad (7)$$

with $n(\overrightarrow{x})$ defined as the refraction index and s the geometric position along the path. Let us choose an initial field $n_0(\overrightarrow{x})$. This initial field is used as a reference, and may or may not be vacuum. The corresponding total optical length, if the propagation took place through $n_0(\overrightarrow{x})$ would be:

$$L_0 = \int_{p_0} n_0(\overrightarrow{x}) ds \qquad (8)$$

L_0 will differ from L due both to a geometrically different path p_0, and a different speed of light along the path. However, $n_0(\overrightarrow{x})$ is known, which allows us to evaluate trajectories numerically over it.

Given some observations, the differences $L_{obs} - L_0$ for each ray contain some information concerning the errors in having assumed the field $n_0(\overrightarrow{x})$ as an approximation to $n(\overrightarrow{x})$. Given an array of many different configurations, and thus many trajectories over

the same field, this allows to perform some kind of tomographic reconstruction of the field. This tomographic approach was taken by Flores et al. (2001), under the assumption of straight line propagation, equivalent to use a constant field, such as vacuum, as the reference field $n_0(\vec{x})$. Alternatively, we may also interpret it as an assumption that,
5 even if the field is not zero, that only the difference in speed is relevant, whereas the geometric difference of the paths through the fields n_0 and n would be negligible.

In this study, we consider instead geometrical configurations where the bending of the ray is relevant and non-zero, but small (around 1°). A substantial fraction of the excess optical path is therefore geometric, since the trajectory is not a straight line.
10 From the two reasons why the optical lengths L and L_0 differ (different geometric length and different refraction index) we will assume that we have an initial field n_0 that is sufficiently close to the actual one n, so that the error in the length of the trajectory is indeed negligible. This can be justified from the following. The geometric optics trajectory, which is representative of the propagation even in a wave optics evaluation,
15 as it is the center of the propagation beam, is a stationary trajectory, usually minimal, of the optical path between the emitter and receiver, when comparing neighbouring paths p. In functional terms, this is expressed as a stationary condition:

$$\frac{\delta L}{\delta p} = 0 \tag{9}$$

Therefore, around a stationary trajectory of the unknown field n, there is a wide band
20 of trajectories whose optical path over n is very similar. It is therefore the region where it is less critical that instead of the true path p, we know only p_0. Comparing the optical paths over two differing fields n_0 and n:

$$\frac{\delta L}{\delta n} = \frac{\partial L}{\partial n} + \frac{\delta L}{\delta p}\frac{\partial p}{\partial n} \tag{10}$$

The variation of the optical length with a change in the propagation field (left hand side)
25 is composed of the purely optical part, at constant trajectory (first term of the right

hand side), and a geometrical term (second term) due to the change of the trajectory. However, the second term is null *if the trajectory was stationary*.

This means that we can evaluate the optical length of stationary trajectories over fields other than the known n_0, without having to evaluate the geometric variation of the trajectory, as long as we do not exceed the linear regime. This allows us to search for the true field n in the (hugely dimensional) space of possible refractivity fields, having evaluated the geometrical shape in only one of these fields, i.e. n_0.

Propagation equation

The eikonal propagation equation plays a major role in geometrical optics and can be considered as the basic equation of geometrical optics. The derivation of the eikonal equation from the Maxwell equations can be found in Born and Wolf (1980). The solution of the eikonal equation gives the geometrical wavefronts of the propagating electromagnetic waves. It expresses the field L of local phase delays through the space, with respect to the phase of the source. That corresponds to the optical path from the source to any other point in space:

$$(\nabla L)^2 = n^2 \tag{11}$$

with n the field of refraction index. The propagation takes place orthogonally to the isosurface of the optical paths. We need to integrate a ray path which is a line always tangent to ∇L.

4.2 Optical path length variation function of refractivity field

The quantity we want to obtain is the inaccuracy $\varepsilon_n(\vec{x})$ of the guessed refraction index. The inaccuracy of the optical path of a given ray can be expressed to first order as:

$$\delta L = \frac{\delta L}{\delta n(\vec{x})} \, \delta n(\vec{x}) + \frac{\delta L}{\delta p} \frac{\delta p \, [n]}{\delta n(\vec{x})} \, \delta n(\vec{x}) \tag{12}$$

The first term expresses the speed term of the optical path, the second one the geometric dependence. Due to stationary trajectory the second term vanishes. The above expression reduces to:

$$\varepsilon_{\mathrm{L}} = \frac{\delta L}{\delta n(\vec{x})}\, \varepsilon_n(\vec{x}) \tag{13}$$

4.2.1 Variational Calculus theory

In variational calculus we however do not want to find a minimum of a function, but rather a function that minimizes an integral. With boundary conditions determined by the positions of the transmitter and receiver, the path with least time delay can be obtained by solving a second order ordinary differential equation. However, due to the variable coefficients and nonlinearity of the equation, care needs to be exercised in the process of the solution. Ray tracing algorithm suggests to use an iterative approach based on the differential form of Snell's law to find the curved ray paths as explained hereafter.

4.2.2 Variational principle in geometrical optics

As Fermat principle states: the time taken for an actual path traced by a ray of light is an extremum. Cartheodory's theorem mentionned that it was a true minimum and established the connection between the Fermat principle and the calculus of variations defining precise extremals (Caratheodory, 1937). This theorem conducts to a fundamental principal of geometrical optics: optical path length of any ray is a minimum. Therefore, the path of a ray can be found minimizing the optical path length. This minimization will give the path of the wavefront in an optical medium of refractive index n. This can be expressed as:

$$\frac{\delta}{\delta p} \int_p n\, ds = 0 \tag{14}$$

The solution to this functional equation also follows an associated Euler set of differential equations (Gelfand and Fomin, 2000; Born and Wolf, 1980). The systems of differential equations and boundary conditions are summarized below:

Differential equations (S_1): $\begin{cases} \frac{d^2 x_i}{ds^2} = \frac{1}{n}\left[\frac{\delta n}{\delta x_i} - \frac{dn}{ds}\frac{dx_i}{ds}\right] \\ \frac{dL}{ds} = n \end{cases}$

5 Where s is the geometrical path along the trajectory.

Boundary conditions (S_2): $\begin{cases} \overrightarrow{x_0} = \overrightarrow{x_{GPS}} \\ \overrightarrow{x_F} = \overrightarrow{x_{LEO}} \\ L_0 = 0 \end{cases}$

0 and F express the initial and final points of the trajectory.

The solution to the system of differential equations S_1 delivers the ray trajectory and the optical path length. In order to realize the inversion and retrieve the refraction index field, we must extract from the obtained ray trajectories which region of the atmosphere 10 is participating in the propagation of every ray and compare the observed and predicted delays.

5 Inversion procedure to retrieve refractivity field

After having detailed the theoretical part, we describe here the inversion procedure 15 used to extract the refractivity field using GPS-RO data. The raytracing procedure, as a tomographic one, may allow in principle to extract three-dimensional information. However a full three-dimensional solution would require massive amounts of data, which generally will not be available. We restrict, then, to the case of a quasi-spherical solution, which is only a function of the altitude over the mean sea level. To realize the 20 inversion procedure that leads to the refractivity field we explore here two possibilities.

The first specifies a one-dimensional solution space, consisting in a uniparametric family of refractivity fields, that contains our reference field. Since the solution space

is small, we may explore it explicitly, launching several series of raytraces, over several members of this uniparametric family of fields.

The second is perturbative. It considers a substantially larger solution space, from a multidimensional family of fields. This space of possible fields is vastly larger, and can-

5   not be explored in search for a solution explicitly. We will then use ancillary information collected during the raytracing over only one field, to describe propagation properties in the neighbourhood of the guess field n_0. The neighbourhood is only described to the linear level of departure from the guess field. The solution is selected through a least squares procedure.

10   As done in Cardellach et al. (2004) we consider a univariational solution space. In this case, the family of field solutions differs uniformly by a small fraction with respect to the reference field. We can afford the simulation exercise of exploring explicitly the family for several values of this fraction. This is done to assess the potential sensitivity of a reflection observable in case of RO event to detect the variations in tropo-

15   spheric parameters (Cardellach et al., 2010). The experiment has been run defining the reflection-observable as the carrier-phase delay between the reflected radio-link and the direct one with a formal precision of the order of a few-centimeters. The ray tracer detailed previously is used to track both direct and reflected signals. An ECMWF refractivity profile is used, with 6 other atmospheric profiles modified by applying a

20   1% reduction to the refractivity below 5 km altitude. Then the corresponding simulated reflection-observable is generated. In total we got 7 profiles that are shown in Fig. 5. The figure also shows the interferometric phase from the reflection that appears in COSMIC occultation C001.2006.227.00.46.G02. The set of 7 profiles show that a 1% variation in the lowermost layers of the troposphere introduces between 0.2 to 0.75 m

25   variation in the carrier-phase delay, larger than the formal error of the observables (see errorbars in the in-set of Fig. 5). This academic exercise does not take into account the variation of refractivity from one layer to another. Of course, the main issue of this technique is to determine which modeling variation space would be better.

In the second procedure we consider a multidimensional solution space. The solution allows a series of independant layers with different refractivity index respectively (Fig. 6). A least squares procedure, described below, finds the best solution within this space.

5.1 Least squares method and inversion procedure

From the obtained ray trajectories issued from the so-called OAT ray-tracer model (Aparicio and Rius, 2004) prepared to track both direct and reflected signals, we must determine which regions of the atmosphere divided in finite elements are participating in the propagation of every ray. Next, we compare the predicted and the observed delays. The ray tracing delivers a prediction for the observable delay L^0 under different atmospheric conditions. Then we attribute a weight w_{rj} to each finite element proportional to its contribution to the excess optical path length. Using the weight matrix and the phase observation difference it is possible to deduce the refraction index correction (linear least squares) responsible for the difference between measured and evaluated delays.

What we know from the ray tracing is a prediction of an observed delay L^0 that can be decomposed as follows:

$$L^0 = l^0 + g^0 + a^0 \tag{15}$$

With l^0 the straight line delay, g^0 the excess geometric delay due to ray bending and a^0 the atmospheric delay. We can calculate with very high accuracy the delay l^0 thanks to the positions of the emitter and receiver.

If we decompose the reference atmospheric field n_0 into finite elements, which we will assume as a number of quasi-spherical shells bounded by surfaces of constant altitude over the mean sea level, the analysis of the ray tracing can also deliver the contribution of each finite element to a^0. This corresponds to the optical length $\int [n_0(\vec{x}) - 1] ds$ accumulated along the trajectory within the element.

Then, we can define for every ray a weight w to each finite element proportional to its contribution to the excess optical length. The result is an ensemble w_{rj}, that is, the exess optical length to ray r that accumulated while it was propagating into the finite element j. Thus the atmospheric delay for each ray can be expressed as follows:

$$a_r^0 = \sum_j w_{rj} \tag{16}$$

If we have measurements L_r^{obs} of the path delays L_r, we can use a minimization approach to obtain the most probable error field in our assumed refractivity. To describe these errors we express a list of unknown relative errors ε_j in our knowledge of the refractivity in each finite element. We get:

$$N_j = N_j^0 \left(1 + \varepsilon_j\right) \tag{17}$$

The difference between the reference and actual paths delays can be expressed as follows:

$$L_r - \left(l_r^0 + g_r^0\right) = \sum_j w_{rj} \left(1 + \varepsilon_j\right) \tag{18}$$

Then the observationnal measurement taking into account the observationnal error e_r becomes:

$$L_r^{obs} - \left(l_r^0 + g_r^0\right) = \sum_j w_{rj} \left(1 + \varepsilon_j\right) + e_r \tag{19}$$

This expression can be expressed in a matrix form as:

$$\overline{\Delta L} = \overline{W} \, \varepsilon + \overline{E} \tag{20}$$

To solve the Eq. (20) optimally we use a least squares method. The ensemble E of measurement errors is unknown. So we solve the matrix expression as $\overline{\Delta L} = \overline{W} \varepsilon$.

Consequently, the solution to ε contains some errors caused by having neglected the measurement errors, as well as model errors. GNSS measurements contain millimeter-order errors and are therefore neglected. Model errors can be related to the homogeneity in the finite element cells or in the modelization of geometric optics, atmospheric and ionospheric scintillation, or in position errors of the emitter or the receiver. We will here assume that model and position errors are small. To find the least squares solution of Eq. (20), we construct the system of normal equations as explained in Golub (1965): $\overline{W}^T \overline{\Delta L} = \overline{W}^T \overline{W} \varepsilon$. This sytem of equations can be solved to:

$$\varepsilon = \left(\overline{W}^T \overline{W} \right)^{-1} \overline{W}^T \overline{\Delta L} \tag{21}$$

Thus, we get the most probable solution ε as a least squares solution and also the corresponding covariance matrix $C = s_0^2 (\overline{W}^T \overline{W})^{-1}$. This solution can be interpreted as the fractional deviations of the solution refractivity field with respect to the reference field. The scale factor s_0^2 is equal to $v^T v / f$, with v the vector of residuals, and f the number of degrees of freedom of the fit.

Therefore, the ray tracing has been used to record the contribution of each finite element to each ray. The least-squares procedure delivers the most probable error field of the guess and the covariance matrix of the result.

5.2 Selection of observables for the inversion

In the former section, we have considered some hypothetical observables of optical path, which may have been gathered over an array of paths. Actual observables are not directly any optical path, but rather combinations of several optical paths, along several trajectories. In particular, we have extracted unwrapped phases over the direct and reflected paths. These phases are not optical paths, but differences between optical paths. However, this does not change the least squares procedure of inversion, as these are linear combinations of the system of equations $\overline{\Delta L} = \overline{W} \varepsilon$.

The original system is based on the output of the raytracing. We may simply combine linearly this system according to the observables that we actually have. In addition, given that we are analyzing the reflected signal, and that we have extracted it through its interference with the direct signal, therefore essentially extracting the relative phase between both: our observable will be the difference between the optical lengths through the direct and reflected propagation paths. This difference is of course a linear combination of two of the raytracings.

We then have a ray tracing function, such as: $f(n) = L$

Then, applying the derivative we get:

$$f(n) = f_0(n_0) + W(n - n_0) \tag{22}$$

with n_0 as a reference field, and W is the ensemble of dependences, which, as shown above, depend only on the optical excess lengths, but not on the geometric difference of the trajectory. An equation of the following kind, expresses the relationship between the error of the field, and observables: $W \Delta n = \Delta \varphi$

Where W stems from the raytracing. Then, the least squares method is used to solve the equation and the final equation to solve becomes:

$$\Delta n = \left(W^T W\right)^{-1} W^T \Delta \varphi \tag{23}$$

5.3 Ray tracing exemples with real data from COSMIC

In this study we use COSMIC data, the atmospheric and ionospheric profiles are available from the radio occultation itself, as well as ECMWF guess fields.

The raytracer estimates over several guess fields the trajectories of the rays. In order to analyze where is actually located the additional information of the reflected signal, we represent here both direct and reflected length paths along an occultation event (Fig. 3). We plot the 300 m band around the different signals to show the available information received from the GPS correlator. The new information brought by the reflected signal is depicted between 45 to 65 s.

Next, a comparison on the difference between path calculated from real data ("measured") and evaluated by the ray tracing is done. The "measured" one corresponds to the interferometric unwrapped phase. The evaluated path length is estimated over five guess fields declined as follows:

5   1. The use of an exponential atmosphere (labeled STD) that is a simple model $N = 300 \exp^{\frac{-h}{H}}$ with, $H = \frac{15 \text{ km}}{\log(10)}$, without ionosphere.

2. The exponential atmosphere above (STD), but adding a ionosphere as given by the COSMIC estimation

3. ECMWF guess field, without ionosphere

10   4. ECMWF guess field, with ionosphere as extracted by COSMIC

5. A reference vacuum ray tracing (straight lines)

Whenever the ionosphere is present, the ionospheric refractive index is evaluated for the L1 frequency, as only the L1 interferometric phase had been extracted. The comparison is shown on Fig. 7. Black curves did not used ionosphere correction.
15 The red curves using the ionosphere correction show closest results to the measured interferometric phase that is issued from real data.

In the next two figures, we show the result of the two procedures mentioned in search for a solution: uniparametric exploration, or multidimensional solution by perturbation analysis and least squares optimization. We find that the experimental data is of suffi-
20 cient quality to constrain the solution to useful levels.

6   Conclusions

We can see that the interferometric unwrapped phase is very close to the corresponding quantity as evaluated over a numerical guess field. The fields that are likely to be of superior quality (ECMWF, ionosphere included), are closer. Furthermore, the precision of the interferometric observables is much finer than the effects of 1% variations in the atmospheric profiles. Firstly, this supports that the interferometric unwrapped phase is a potentially useful observable, that is recoverable and potentially used. The observable is quantitatively extracted with high accuracy, supporting its potential.

Secondly, the raytracing allows the interpretation of this observable data providing the elements to choose a solution within the space of refraction index fields neighbouring the guess field. A search in a layered space of 20 dimensions (i.e. there were 20 low tropospheric layers, each allowed to vary independently) showed that the level of constrain is sufficient to be useful.

This study was a first attempt to evaluate the reflected signals potentiality in terms of tropospheric information content. In this paper we introduced the way the reflected signals occuring during an occultation event could be extracted from the direct one. Signal separation was conducted using radio-holographic analysis. Then the spectral content of each signal was interpreted computing the direct and indirect phase.

Later on, the relative delay between the reconnected direct and indirect signals had been deduced. After these steps of extraction the interpretation contained in the signal has been shown. The ray tracing procedure has proven its ability to invert travel-time data to a refractivity field.

The ray-tracer model allows to track both direct and reflected signals. As demonstrated in the sensitivity study made in Sect. 5, the tropospheric information content is embedded in the RO reflected signals. In addition, we have shown that reflection-observables are able to capture variations in the tropospheric profile. This ability to sense and refine the variations in the troposphere would be of great interest to improve the tropospheric information content in near-surface.

We have shown that it is possible to do realistic ray tracing thanks to the comparison between measured unwrapped phase and over realistic refractivity models. The comparison has been done taking into account the ionospheric state. The computation of the non-vacuum ray tracing methods have shown to be reasonably close to the
5 unwrapped reflected phase. Also, the least squares inversion allows the extraction of useful meteorological information. After having highlighted the potential of GPS-RO reflected signals to sense the lowermost layers of the troposphere. The main perspective of the work consists in determining the ability of such a measurement to quantify the properties of the low atmosphere (refractivity profile within the boundary layer).
10 If the determination of such properties is feasible then the Numerical Weather Forecast system of Environment Canada could take advantage of the RO-observations. In addition, we remind that RO measurements is a uniform worldwide sampling and an all-weather measurement technique. Also these measurements can greatly improve Southern Hemisphere data particularly near tropopause. All these advantages pro-
15 vided by the RO measurement technique are valuable to improve data assimilation experiments.

References

Ao, C., Meehan, T., Hajj, G., Mannucci, A. J., and Beyerle, G.: Lower troposphere refractivity bias in GPS occultation retrievals, J. Geophys. Res., 108, 4577, 2003. 1201
Aparicio, J. M. and Deblonde, G.: Impact of the Assimilation of CHAMP Refractivity Pro-
25 files on Environment Canada Global Forecasts, Mon. Weather Rev., 136, 257–275, doi:10.1175/2007MWR1951.1, 2008. 1202

Aparicio, J. M. and Rius, A.: A raytracing inversion procedure for the extraction of the atmospheric refractivity from GNSS travel-time data, probing the Atmosphere with Geodetic Techniques, Phys. Chem. Earth A/B/C, 29, 213–224, doi:10.1016/j.pce.2004.01.008, 2004. 1215

Beyerle, G. and Hocke, K.: Observation and simulation of direct and reflected GPS signals in Radio Occultation Experiments, Geophys. Res. Lett., 28, 1895–1898, 2001. 1204, 1205

Beyerle, G., Hocke, K., Wickert, J., Schmidt, T., Marquardt, C., and Reigber, C.: GPS radio occultations with CHAMP: A radio holographic analysis of GPS signal propagation in the troposphere and surface reflections, J. Geophys. Res., 107(D24), 4802, doi:10.1029/2001JD001402, 2002. 1201, 1202, 1205

Born, M. and Wolf, E.: Principles of optics: Electromagnetic theory of propagation, interference and diffraction of light, Pergamon Press, London, 1980. 1211, 1213

Caratheodory, C.: Geometrische Optik, Springer, Berlin, 1937. 1212

Cardellach, E., Ao, C. O., de la Torre Juárez, M., and Hajj, G.: Carrier phase delay altimetry with GPS-reflection/occultation interferometry from low Earth orbiters, Geophy. Res. Lett., 31, 133–143, 2004. 1203, 1214

Cardellach, E., Oliveras, S., and Rius, A.: Applications of the Reflected signals found in GNSS Radio Occultation Events, in: Proceedings of GRAS SAF Workshop on Applications of GPS radio occultation measurements, 133–143, 2008. 1201, 1202

Cardellach, E., Oliveras, S., and Rius, A.: Correlation between tropospheric variables and GNSS radio-occultation reflected signals, Radio Sci., submitted, 2010. 1204, 1214

Cucurull, L., Kuo, Y.-H., Barker, D., and Rizvi, S. R. H.: Assessing the Impact of Simulated COSMIC GPS Radio Occultation Data on Weather Analysis over the Antarctic: A Case Study, Mon. Weather Revi., 134, 3283–3296, doi:10.1175/MWR3241.1, 2006. 1202

Fjeldbo, G., Kliore, A. J., and Eshleman, V. R.: The neutral atmosphere of Venus as studied with the Mariner V radio occultation experiments, Astronom. J., 76, 123–140, 1971. 1200

Flores, A., Rius, A., Vilà-Guerau de Arellano, J., and Escudero, A.: Spatio-Temporal Tomography of the Lower Troposphere Using GPS Signals, Phys. Chem. Earth, 26, 405–411, 2001. 1210

Gelfand, I. and Fomin, S.: Calculus of Variations, Dover Publ., 2000. 1213

Golub, G.: Numerical methods for solving linear least squares problems, Numer. Math., 7, 206–216, 1965. 1217

Title Page

Abstract | Introduction

Conclusions | References

Tables | Figures

◄◄ | ►►

◄ | ►

Back | Close

Full Screen / Esc

Printer-friendly Version

Interactive Discussion

Gorbunov, M.: Accuracy of the refractometric method in a horizontally nonuniform atmosphere, Izv., Atmos. Ocean. Phys., 5, 381–384, 1988. 1200

Gurvich, A., Kan, V., Popov, L., Ryumin, V., Savchenko, S., and Sokolovskiy, S.: Reconstruction of the atmosphere's temperature profile from motion pictures of the Sun and Moon taken from the Salyut-6 orbiter, Izv., Atmos. Ocean. Phys., 1, 7–13, 1982. 1200

Hajj, G., Ibanez-Meier, R., Kursinski, E., and Romans, L.: Imaging the ionosphere with the global positioning system, Int. J. Imag. Syst. Tech., 5, 174–184, 1994. 1200

Healy, S.: Assimilation of GPS radio occultation measurements at ECMWF, in: Proceedings of GRAS SAF Workshop on Applications of GPS radio occcultations measurements, 99–109, 2008. 1202

Hocke, K., Pavelyev, A. G., Yakovlev, O. I., Barthes, L., and Jakowski, N.: Radio occultation data analysis by the radioholographic method, J. Atmos. Sol.-Terr. Phy., 61, 1169–1177, doi:10.1016/S1364-6826(99)00080-2, 1999. 1203, 1204

Kursinski, E. R., Hajj, G. A., Bertiger, W. I., Leroy, S. S., Meehan, T. K., Romans, L. J., Schofield, J. T., McCleese, D. J., Melbourne, W. G., Thornton, C. L., Yunck, T. P., Eyre, J. R., and Nagatani, R. N.: Initial Results of Radio Occultation Observations of Earth's Atmosphere Using the Global Positioning System, Science, 271, 1107–1110, doi:10.1126/science.271.5252.1107, 1996. 1200

Melbourne, W. G.: Radio occultations using Earth satellites: A wave theory treatment, vol. 6 Monograph, Deep space communications and navigation series, jet propulsion laboratory california institute of technology edn., Wiley Inter Science, 2004. 1204

Parkinson, B. W. and Spilker, J. J.: Global Positioning System: Theory and Applications, vol. 1, American Institute of Aeronautics, 1996. 1205

Pavelyev, A., Volkov, A., Zakharov, A., Krutikh, S., and Kucherjavenkov, A.: Bistatic radar as a tool for earth investigation using small satellites, Acta Astronaut., 39, 721–730, doi:10.1016/S0094-5765(97)00055-6, 1996. 1204

Poli, P.: Preliminary assessment of the scalability of GPS radio occultations impact in numerical weather prediction, Geophys. Res. Lett., 35, L23811, doi:10.1029/2008GL035873, 2008. 1202

Raymund, T., Austen, J., Franke, S., C.H. L., and Klobuchar, J.: Application of computerized tomography to the investigation of ionospheric structures, Radio Sci., 25, 771–789, 1990. 1200

Meteorological information in GPS-RO reflected signals

K. Boniface et al.

Rennie, M. P.: The impact of GPS radio occultation assimilation at the Met Office, Q. J. Roy. Meteor. Soc., 136, 116–131, doi:10.1002/qj.521, 2010. 1202

Rocken, C., Kuo, Y.-H., Schreiner, W., Hunt, D., Sokolovskiy, S., and McCormick, C.: COSMIC System Description, Terr. Atmos. Ocean. Sci., 11, 21–52, 2000. 1203

5 Sokolovskiy, S.: Solution of the inverse refraction problem by sensing of the atmosphere from the space, Sov. J. Remote Sens., 3, 333–338, 1990. 1200

Sokolovskiy, S., Rocken, C., Schreiner, W., Hunt, D., and Johnson, J.: Postprocessing of L1 GPS radio occultation signals recorded in open-loop mode, Radio Sci., 44, RS2002, doi:10.1029/2008RS003907, 2009. 1201

Meteorological information in GPS-RO reflected signals

K. Boniface et al.
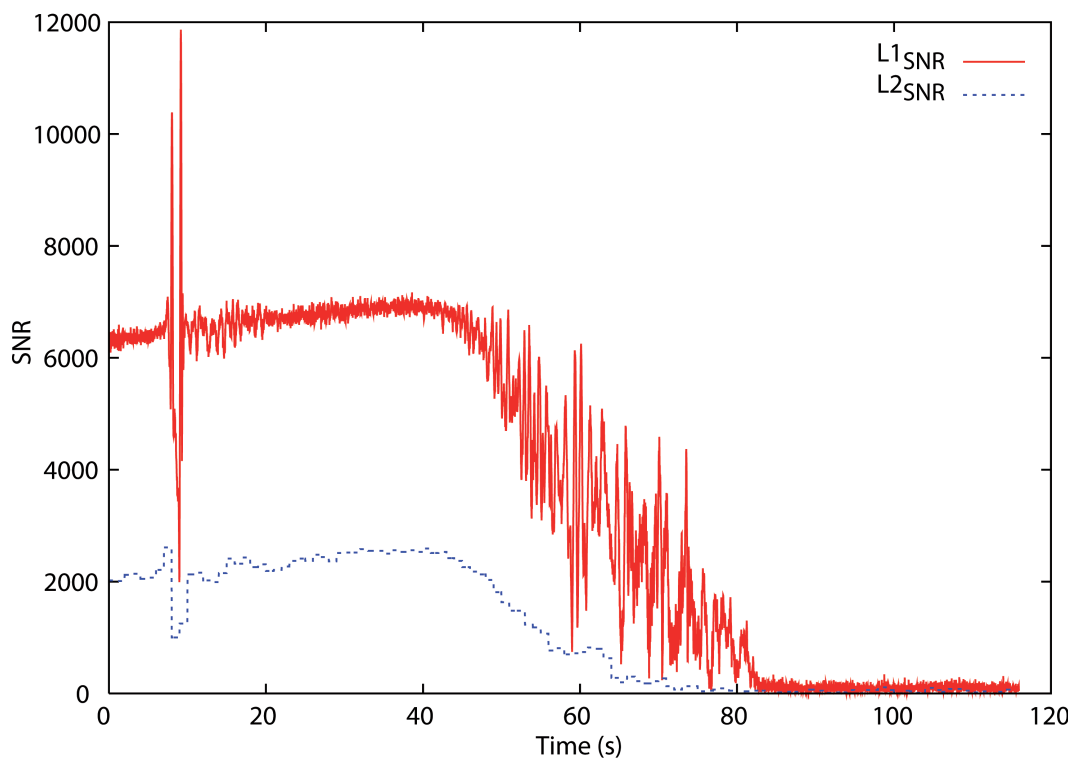
Fig. 1. Signal to Noise Ratio (SNR) on the L1 and L2 channels. Each SNR is given in 1/10 volts/volt. COSMIC Data are provided by the University Corporation for Atmospheric Research (UCAR). Beyond 80 s the signal is note enough powerful to be considered.

Title Page

Abstract | Introduction

Conclusions | References

Tables | Figures

◄◄ | ►►

◄ | ►

Back | Close

Full Screen / Esc

Printer-friendly Version

Interactive Discussion

Full Screen / Esc

Printer-friendly Version

Interactive Discussion
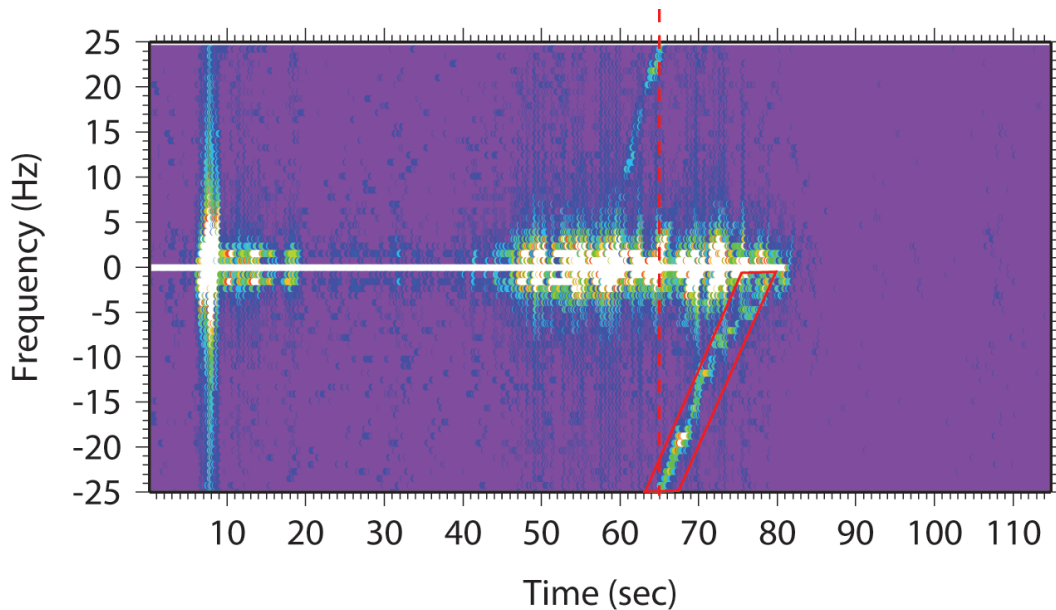
Fig. 2. Temporal evolution of radio hologram power spectrum derived from GPS occultation on 10 April 2007 at 00:29 h (COSMIC-1 data file: atmPhs_C001.2007.100.00.29.G05_2007.3200). The red parallelogram represents the complementary mask that has been formed ad hoc to detect the reflective part of the signal. The mask is centered at 65 s with a slope of 0.52.

Meteorological information in GPS-RO reflected signals

K. Boniface et al.
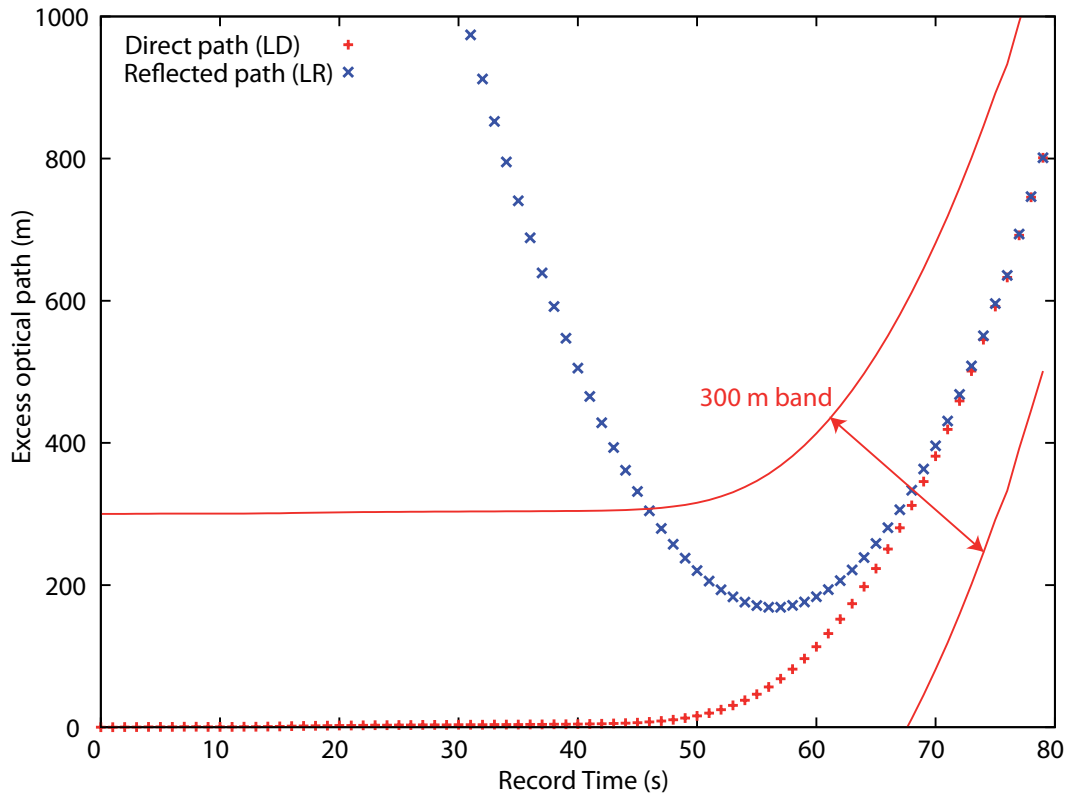
Fig. 3. Direct and reflected excess optical paths (m). The 300 m band represents the range of delays when the reflected signal will be captured by the correlator that tracks the direct signal, and interfere with it.
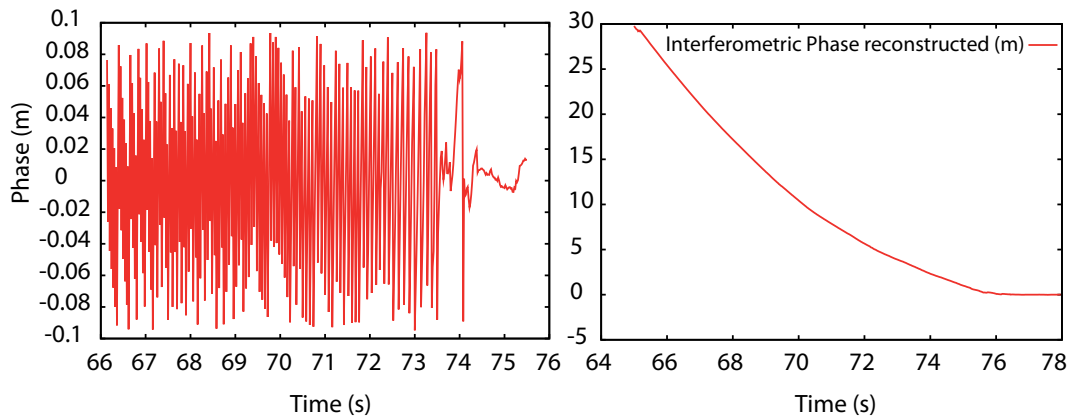
Fig. 4. Phase difference between the reference signal and the reflected signal (left). This phase difference can also be unwrapped removing the 2π jumps to get the interferometric phase (right).
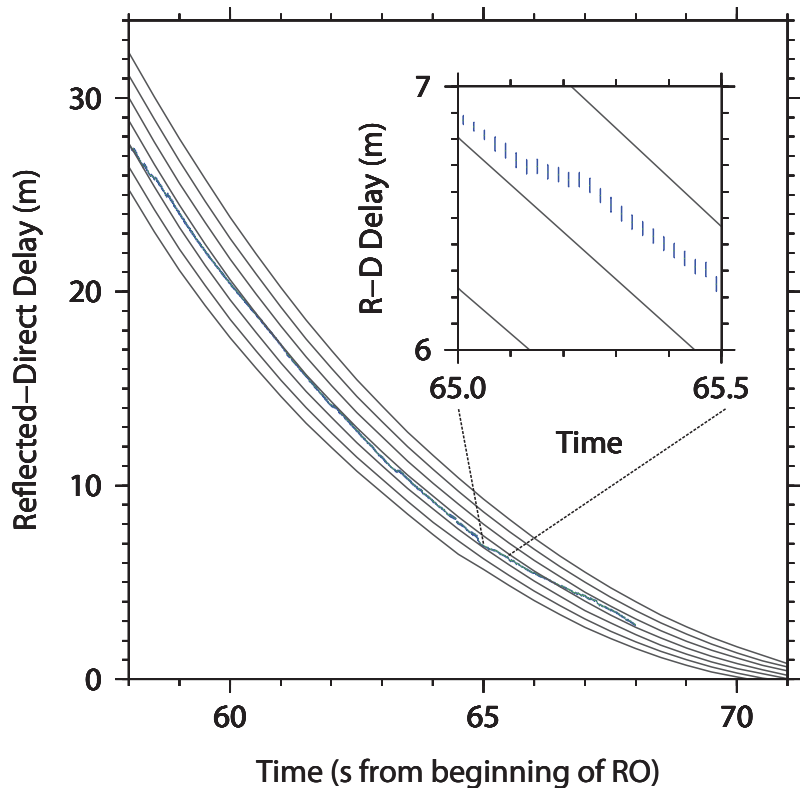
Fig. 5. Comparison between the real data COSMIC's C001.2006.227.00.46.G02_2006.3200 interferometric delay (observables with error bars) and the ray tracer simulated observables based on the ECMWF atmospheric profile. A 1-dimensional family of profiles is prepared reducing the refractivity below 5 km. The figure shows the profiles with 0.94, 0.95, ... 1.00 times the ECMWF refractivity. Observables simulations with OAT allow to assess the potential sensitivity of reflection RO events to extract tropospheric profile variations. The reflection appears in COSMIC GPS occultation on 15 August 2006 at 00:46 h.
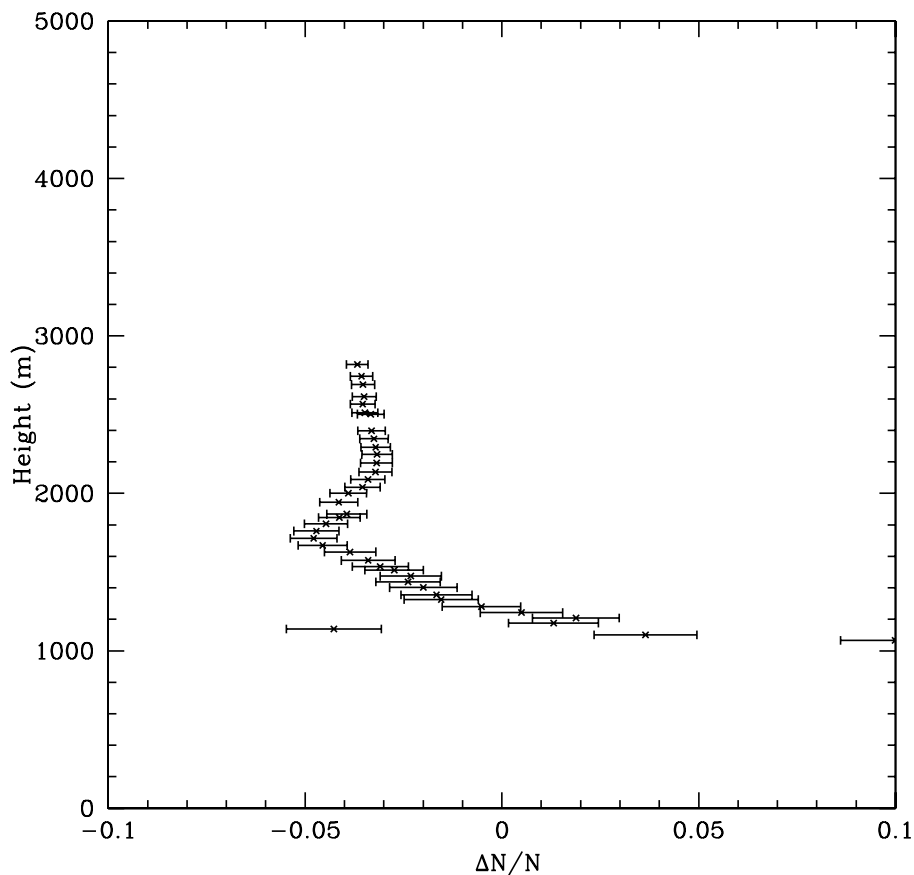
Fig. 6. Refraction index correction coefficients ($\frac{\Delta n}{n}$) to the ECMWF profile. A multidimensional solution space has provided this solution. It allows a series of independant layers with different refractivity index respectively.
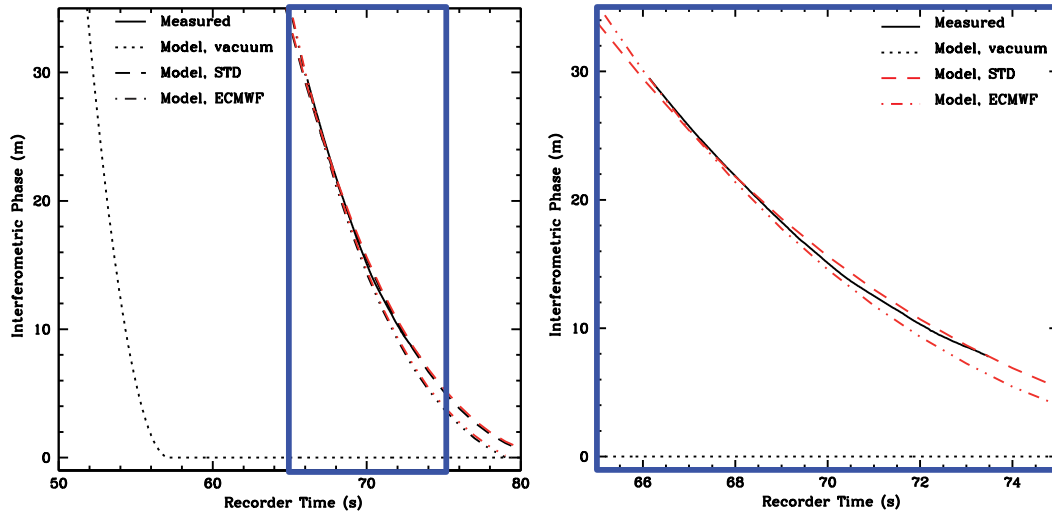
Fig. 7. Path difference between direct and reflected signals over sea using interferometric phases measured and evaluated with raytracing. Black evaluated curves do not use ionosphere correction. Red evaluated curves use COSMIC's estimation. On right hand side a zoom of the same path difference is shown.